Research Square

Preprints are preliminary reports that have not undergone peer review.
They should not be considered conclusive, used to inform clinical practice,
or referenced by the media as validated information.

Spatio-temporal clustering of successive earthquakes: analysis of a global CMT catalog.

Thystere Matondo Bantidi (bantidi1@dc.tohoku.ac.jp)
Tohoku University https://orcid.org/0000-0002-2435-8854
Takeshi Nishimura
Tohoku University

Full paper

Keywords: Spatio-temporal clustering, successive occurrence, triggering distance, Coulomb stress change

Posted Date: March 30th, 2020

DOI: https://doi.org/10.21203/rs.3.rs-19718/v1

License: This work is licensed under a Creative Commons Attribution 4.0 International License.
Read Full License

Spatio-temporal clustering of successive earthquakes: analysis of a global CMT catalog.

Thystere Matondo Bantidi,

Department of Geophysics, Graduate School of Science, Tohoku University

6-3 Aramaki-aza Aoba, Aoba-ku, Sendai, 980-8578, Japan,

bantidi1@dc.tohoku.ac.jp

Author #2: Takeshi Nishimura,

Department of Geophysics, Graduate School of Science, Tohoku University

6-3 Aramaki-aza Aoba, Aoba-ku, Sendai, 980-8578, Japan

takeshi.nishimura.d2@tohoku.ac.jp

Corresponding author: Thystere Matondo Bantidi

Abstract

Spatio-temporal clustering of seismicity features is an interesting phenomenon that is relevant for earthquake generation process and operational earthquake forecasting. We analyze successive earthquakes that closely occur in space and time in order to clarify how large earthquakes successively occur. We use the Global Centroid Moment Tensor catalog for the period from 1976 to 2016. Shallow earthquakes with a moment magnitude, M_w, of larger than or equal to 5.0 are analyzed. We first sort all of the earthquakes in time to select a master event from the beginning. Then, we group the earthquakes that occur within a horizontal distance (D) and a lapse time (T_a) from the master event into a cluster. Next master event is selected from the catalog in order, and the same procedure is repeated. We count the number of the clusters, which represent the successive earthquakes, for different D and T_a. To examine whether or not successive earthquakes randomly occur, we compare the results with simulations in which earthquakes are set to occur randomly in time but at the locations same with the estimated centroid. The results show that the cumulative numbers of clusters for the simulation more rapidly increase with the horizontal distance than those for real data at short distance ranges, and the formers approach to the latter at long distance range. The triggering distance, at which the cumulative numbers of real and simulation data merge, increases with increasing the magnitude of master event. The triggering distance becomes smaller as the lapse time increases, which implies that the seismic activity turns to become the normal condition in which the occurrence time intervals of large earthquakes obey a Poisson distribution. The triggering distance increases with being almost proportional to the 1/3 of the seismic moment of master earthquake, and the number of earthquakes occurring in the region with positive Coulomb stress change (ΔCFF) are more than 60-80% of the total number of the successive earthquakes. These results suggest that static stress change introduced by a master event is one of the triggering mechanism of successive earthquakes.

Key words: Spatio-temporal clustering, successive occurrence, triggering distance, Coulomb stress change.

1. Introduction

Some earthquake forecasting models are rooted in the idea that earthquakes can generate other earthquakes and the triggering probability depends on space, time, and magnitude. A well-known classical empirical scaling law is Omori law, which states that the occurrence rate of earthquakes after a large earthquake (i.e., mainshock) decays with being proportional to t^{-p} where t is the time and p a constant of about 0.7 – 1.1 (Utsu, 2002). Also, Gutenberg-Richter's law (Gutenberg and Richter, 1944), which describes the magnitude-frequency distribution of earthquakes, is used in these methods. Another empirical law, Bath law, is also important to understand the occurrence of earthquakes after a large earthquake, which shows that the magnitude of the largest aftershock is about 1.2 less than that of the main shock (Bath, 1965). For these decades, seismologists have investigated the spatio-temporal distribution of seismicity based on these empirical characteristics. For example, epidemic type aftershock sequence model (ETAS model; Ogata, 1998), which is based on the Omori law, Gutenberg-Richter law and an idea that an earthquake generates a cluster of offspring earthquakes, has been applied to the earthquakes at many regions to understand the regional or general characteristics of seismicity and to evaluate the seismic hazard (e.g, Console and Murru, 2001; Helmstetter and Sornette, 2002; Ogata and Zhuang, 2006; Kumazawa and Ogata, 2014).

Statistical characteristics of the seismicity is also examined by considering that spatio-temporal distribution of earthquakes is independent of the dimensions of the region under consideration and independent of the seismic magnitude (Kagan and Knopoff, 1980; Corral, 2004a; Marekova, 2014). For instance, at Southern California, where high-quality seismic data are available for recent several decades, both the inter-event distances (distance between earthquakes) and the inter-event times (occurrence time difference between earthquakes) exhibit statistical distributions involving power-law regimes (Bak et al. 2002; Corral, 2004a, 2004b; Corral, 2008; Davidsen and Paczuski, 2005). The statistical characteristics of spatio-temporal distribution of seismicity is often examined by giving a focus on the characteristics of main shock and aftershock sequences (Utsu and Seki, 1954; Utsu et al., 1995; Felzer and Brodsky, 2006; Yukutake and Lio, 2017; Nicole, 2018; Tamaribuchi, 2018). Static or dynamic stress changes is often used to explain these triggered seismicity (Gomberg et al. 1998; Hill et al., 1993; Kilb et al., 2000; Toda et al. 2008, 2011; Freed, 2007)

On the other hand, there are some phenomena that are not well described by the classical laws or ETAS model and/or by the statistical characteristics. For example, it is known that large earthquakes are sometimes preceded by foreshocks: about 10 - 20 % of the main shocks with $M_w \geq 6$ accompany foreshocks (Reasenberg, 1999). But, it is realized again that some of the foreshocks have a magnitude larger than 6, which may severely cause earthquake disasters. For example, in Japan, two days after an M_w7.3 earthquakes, the 2011 Tohoku earthquake with magnitude M_w9.0 occurred along the Pacific plate boundary (Marsan and Enescu, 2012); an M_w6.5 earthquake hit at Hinagu active fault

in Kyushu, Japan, on April 14, 2016, was followed by a large earthquake with M_w7.3 that took place at Futagawa active fault on April 16 (Goda et al., 2016). These large earthquakes may be classified as a foreshock of the following main shock (Utsu, 1954). It is, however, natural that such a large foreshock exceeding magnitude of about 6 is generally recognized as a main shock before the occurrence of the following larger earthquake. It is also known that large earthquakes are sometimes successively observed, which may not be explained by Bath's law and may not be attributed to the classical aftershock activity. For example, along the Anatolian active fault system in Turkey, four large earthquakes with magnitudes of M_w>7.0 successively occurred for the period from 1939 to 1944 and three for the period from 1953 to 1967. For 5 years after the 2004 Sumatra earthquake with an M_w9.2, three large earthquakes with M_w>7 occurred along the plate boundary of Indian oceanic plates and Sumatra Island in Indonesia: the M_w8.7 Nias earthquake on March 28, 2005, which occurred directly to the south of the rupture area of the Sumatra earthquake, the double earthquakes on September 12, 2007, the first M_w8.5 at 11:10:26 occurred about 130 km southwest of Bengkulu on the southwest coast of Sumatra island. On the same day, the second M_w7.9 at 23:49:04 occurred about 205 km northwest of Bengkulu and about 185 km south–southeast of Padang, in West Sumatra.

The present study, therefore, analyzes moderate and large earthquakes to clarify spatio-temporal characteristics of successive earthquakes, which are defined in this study as that the earthquakes occur close to each other both in space and time and may not be attributed to the aftershocks. The present study uses a global earthquake catalog to examine the occurrence probability of another earthquake after a previous one and clarify averaged characteristics of successive earthquakes. The Coulomb stress change (ΔCFF) hypothesis is also examined to understand the generation mechanism of these successive earthquakes. These evaluations can be important not only to understand the earthquake triggering mechanisms but also to prepare for seismic hazards, because the second earthquake can cause severe damages and disaster again in and around the area where a first large earthquake occurs.

2. Data

We use the data catalog of centroid moment tensor (CMT) solutions provided by the Global CMT project operated by Columbia University (Dziewonski, A. M., et al.; 1981; Ekström, G., et al.; 2012). CMT solutions of earthquakes have routinely been determined from analyses of observed seismic waves recorded at stations distributed around the world, and the centroid, occurrence time and moment magnitude of earthquakes occurring around the world are provided. The data for the period of 41 years from 1976 to 2016 are analyzed in the present study. Since CMT solutions are determined for relatively large earthquakes that excite long-period waves propagating in a long-distance, there is no omission in the data catalog for the earthquakes with a magnitude of equal to or larger than about 5.

This can be confirmed from the magnitude frequency distribution that follows Gutenberg-Richter's relation (e.g., Nishimura, 2017). The present study, therefore, gives attentions into the earthquakes with a magnitude larger than or equal to 5.

3. Method for searching successive earthquakes

The present study defines the successive earthquakes as plural earthquakes that occur close to each other both in space and time and are not attributed to the aftershocks. We search such successive earthquakes by using the following steps: (1) Sort the earthquakes in the CMT data catalog in time; (2) a start time is set to be the beginning time of the catalog; (3) A master event with a moment magnitude (M_w) ranging from M_{w1} to M_{w2} is selected in order from the start time. The earthquake is termed as E_o^i, where i represents the number of master event; (4) When an earthquake larger than E_o^i occurs within an interval time of t_b before the occurrence of E_o^i and within a distance of 2000 km from the centroid of E_o^i, E_o^i is unused as a master event, and we go to step 7; (5) The earthquakes satisfying the following two criteria are searched, and are defined as a triggered event belonging to the "cluster" of E_o^i: (i) the earthquake occurs within a lapse time of T_a from the occurrence time of E_o^i; (ii) the horizontal distance from the epicenter of E_o^i is in the range from the minimum distance D_{min} to the distance D; (6) The start time is set to be just after the occurrence time of the i-th master event, and go to step 3 to select a next master event (i+1) which is not belonging to the clusters previously determined; (7) The procedures from steps (3) to (6) are repeated until the last earthquake in the catalog. We define the earthquakes belonging in each cluster as "successive earthquakes".

The time interval, t_b, which is used to remove the main shocks, is set to be 14 days, because most of the largest aftershocks occur within 10 days after the occurrence of each main shock (Utsu, 1957). Following Utsu and Seki (1954), we set the minimum distance, D_{min}, using the following equation : $D_{min} = c\sqrt{A/\pi}$, where A is the slip area in km^2 determined from the magnitude of the master event: $\log_{10} A = 1.02M_w - 4.0$. To sufficiently exclude the aftershocks of master event, we set the coefficient c to be 3. Because the selection of main shocks may change the selection of aftershocks (Felzer and Brodsky, 2006; Marson and Lengliné, 2010), we examine the effect of t_b and/or of c in the following analyses.

Figure 1 illustrates how we define the master events using t_b and D (Steps 3 and 4), and Figure 2 schematically shows how the number of cluster changes with the interval time T_a and the distance D (Step 5). By counting the number of clusters and examining the distributions of cluster in space, we clarify the characteristics of successive earthquakes in the following sections.

4. Results

4.1 Spatio-temporal distributions of successive earthquakes

We divide the earthquakes in the catalog into five magnitude ranges: $5.0 \leq M_w < 5.5$ (25299 earthquakes), $5.5 \leq M_w < 6.0$ (9186 earthquakes), $6.0 \leq M_w < 6.5$ (2753 earthquakes), $6.5 \leq M_w < 7.0$ (931 earthquakes) and $M_w \geq 7.0$ (419 earthquakes). We count the number of clusters for three lapse times (T_a=60, 180 and 365 days). The horizontal distance ranges (D) are also changed: every 10 km from 10 to 500 km for the first two magnitude ranges (M_w<6.0) and every 100 km from 100 to 2000 km for the other magnitude ranges (M_w ≥6.0). Most of cumulative numbers of clusters constantly increase with increasing the lapse time, T_a and with increasing horizontal distance (Figure 3). But, for the magnitude ranges of M_w<6.5, the cumulative numbers of clusters decrease in the ranges of large T_a and/or large D. For example, for $5.0 \leq M_w < 5.5$, the cumulative number begins to decrease from 120 km for all the lapse times. Such decreases are caused by that plural clusters get together by extending the horizontal distance and increasing lapse time.

We may categorize the clusters into two groups: pair-event clusters and multiple-event clusters. The former consists of a master event and another slave event, while the latter is formed by a master event and two or more slave events. For $M_w \geq 7.0$, at least 70% of the clusters are categorized as pair-event clusters at T_a =365 days. The percentage of pair-event cluster decreases with decreasing the earthquake magnitude ranges: 60% for $6.5 \leq M_w < 7.0$ and 38% for $6.0 \leq M_w < 6.5$. In addition, almost half of the clusters show that the master event is followed by one or more slave events with a larger magnitude. For example, for $M_w \geq 7.0$ and at D= 500 km, 8 clusters among 13 ones include larger earthquakes than the master events at $T_a = 60$ days, 12 among 27 clusters at T_a=180 days, and 15 among 39 clusters at T_a=365 days.

4.2 Comparison with the results obtained from random data

Temporal distribution of large earthquakes is well described by a Poisson process when aftershocks are excluded (e.g. Michael, 2011; Shearer and Stark, 2012). Hence, the results shown in the previous subsection may be explained by such a random process, and no triggering mechanism may exist. Here, we analyze simulated data to examine whether the observed successive earthquakes occur randomly, or they are triggered by nearby earthquakes. Simulated data catalogs of earthquakes are generated by randomly changing the origin times of the observed earthquakes while their centroids and magnitudes are fixed (not changed from the observations). That is, the origin times are randomly set for the observation period from 1976 to 2016 by using a random function in a computer code that can generate random values equally distributing between 0 and 1. Then, the numbers of clusters are counted by applying the same procedure as used for the real catalog. The simulations are done 100 times, and the average numbers of clusters are calculated. In Figure 3, the spatio-temporal variation on the cumulative numbers of clusters for simulated catalogs are plotted by dotted lines. The cumulative numbers of clusters for the simulation more rapidly increase with the horizontal distance than those of real data at short distance ranges. The cumulative numbers for the simulated data then approach or

become equal to those for the real data. Alternatively, the numbers of clusters for the real data are always larger than those for the simulated data at shorter distance ranges, and merge to those for the simulated data at long distance ranges. This result strongly suggests that the earthquakes trigger another or more earthquakes in shorter distance ranges. The first intersection point where the number of cumulative clusters obtained from the real data merges with that obtained with the simulated data represents the distance where triggering ceases. We define this distance as "triggering distance". For example, the triggering distances are 200 km and 100 km at $T_a =$ 180 days and $T_a =$ 365 days, respectively, for $6.0 \leq M_w < 6.5$. Those are 300 km and 200 km at 180 and 365 days for $6.5 \leq M_w < 7$, respectively.

Figure 4 plots the triggering distances versus the seismic moment M_o that is calculated from an equation of $M_w = (2/3)(\log M_o - 9.1)$ (Hanks and Kanamori, 1979; Bormann, P., and D. Giacomo, 2010). To convert the magnitude range to M_w, we use the average moment magnitude calculated from all the earthquakes in each magnitude range. The triggering distance increases with increasing the magnitude of master event while the triggering distances decrease with increasing lapse time, T_a. Alternatively, a large earthquake can trigger an earthquake located far from his centroid compared to small earthquakes, and triggering effect gradually diminishes with time around a large earthquake. The triggering distance is almost proportional to 1/3 of the seismic moment.

Table 1 summarizes the percentages of successive earthquakes that occur within a horizontal distance equal to the triggering distances for the all of the observed earthquakes. The percentages for small earthquakes are large compared with those for large earthquakes, as the percentages are about 5 % for $M_w \geq 7$ while those are about 40 % for $5.0 \leq M_w < 5.5$.

Figure 5 plots the locations of the successive earthquakes. It is recognized that these successive earthquakes are distributed not only along subduction zones but also along rift zones. No systematic localization is recognized.

5. Discussion

5.1 Effects of the selection of parameters

Parameters, t_b and c, play a key role in the selection of master events that are used as a first event in each cluster and consequently for the selection of successive earthquakes that belong to that cluster. For example, using smaller c introduce larger numbers of the clusters, and the cumulative numbers especially in the small horizontal distance range are much changed. Hence, the judicious choice of these two parameters must surely help to avoid an overestimation or underestimation of the triggering distance. However, ambiguity remains in the selections of these parameters and there is no robust criterion to define these parameters. In this subsection, therefore, we examine how these two

parameters affect the detection of successive earthquakes and estimation of triggering distances. We analyze the real data by changing t_b from 14 days to 60 days, keeping c=3. We also examine the effects of aftershock area by changing the parameter c from 3 to 1, fixing t_b at 14 days. Figure 4 shows the triggering distances estimated for different t_b and c. The triggering distances for t_b=30 or 60 days are not the same with those for t_b=14 days, but the differences are less than about 10 % at each magnitude range (Figure 4(a)). Similar characteristics are observed for the parameter c (Figures 4 (b)). Decreasing c or increasing t_b does not introduce any significant bias in the estimation of triggering distance. These results strongly suggest that the triggering distance is a stable parameter that is not much affected by the selections of the parameters describing the aftershock activity (i.e., t_b and c).

Using these two parameters (i.e., t_b and c) can reduce the possibility to include so called aftershocks among successive earthquakes. Nevertheless, some aftershocks of a very large earthquake may be contaminated as successive earthquakes in other magnitude ranges. Or, a main shock is defined as a slave event of a foreshock with a large magnitude. For example, the Tohoku earthquake with $M_w9.0$ on March 11, 2011, occurred after a foreshock with $M_w7.3$ on March 9, and are followed by many aftershocks with $M_w \geq 7$. In the case of the magnitude range $M_w < 7.5$, these $M_w \geq 7$ earthquakes are not counted as successive earthquakes, because those earthquakes occurred within a distance less than D_{min} (=741 km) are removed as the aftershocks of the $M_w9.0$ earthquakes by the procedure shown in section 3. But, when the magnitude range is set to be $7 \leq M_w < 9.5$, the $M_w9.0$ is defined as a slave event of the $M_w7.3$ on March 9 with the following slave events ($M_w7.9$ and $M_w7.6$ occurred on March 11, 2011) which must be classified as the aftershocks of $M_w9.0$. However, even if these $M_w7.9$ and $M_w7.6$ are not counted as successive earthquakes, the number of clusters does not change. Also, we have checked that, for the cases in which large earthquakes with $M_w \geq 7$ are followed by other such large earthquakes, the following earthquakes are removed as aftershocks by the procedure section 3.

In Figure 3, the curves of cumulative numbers of clusters for large magnitude ranges and short lapse times are represented by straight lines in log-log plots (power laws), while those for small magnitude ranges and long lapse time tend to show convex shapes. Such difference may be caused by the effect of background seismicity: the background seismicity comes to be dominant as the lapse time increases and/or the magnitude range decreases (Richards, et al., 2010). There is no direct way to exclude such background seismicity effect in our analyses, but the curves of cumulative numbers for the simulated data show similar characteristics. Hence, the estimated triggering distance is considered to be not much affected by the background seismicity.

5.2 Stability of the Simulated data

To measure the triggering distances, we performed 100 times of simulation and obtained averaged cumulative numbers of clusters against the horizontal distance. This makes a stabilized simulation result, but the real data is also just one sample so that the obtained clusters may be a result of fluctuated phenomena. Therefore, to examine how the triggering distances are stably estimated, we evaluate the fluctuation of estimation by measuring the triggering distance by analyzing each simulation data. Figure 6 shows the frequencies of triggering distance obtained from 100 simulated data for T_a =180 and 365 days, c=3 and $t_b = 14$ days. The triggering distances are scattered in a few hundred kilometers, although the peaks of the frequencies are almost matched with the triggering distances obtained from the averages of 100 simulations. As the magnitude or lapse time increases, the scatter seems to become smaller. This suggests that large number of data may decrease the scatter and improve the reliability.

5. 3 Relation to Coulomb stress change

Several mechanisms have been proposed to explain the observed spatio-temporal clustering of earthquakes. Static stress change caused by deformation in the vicinity of a large earthquake may change the Coulomb stress changes on the seismic fault planes (i.g., King et al., 1994; Stein, 1999, Hardebeck et al. 1998; Gomberg, 2005, Toda, 2011). Dynamic stress change associated with the passage of seismic waves excited by a large earthquake is also another possible mechanism to trigger nearby earthquakes (e.g., Felzer and Brodsky, 2006). Viscoelastic relaxation, which is caused by viscous flow in the lower crust or upper mantle after the occurrence of a moderate to large earthquake may also change the stress condition of fault plane (e.g., Freed and Lin, 2001). Large earthquakes may migrate crustal fluids to generate fluid pore diffusion. Such process may decrease the normal stress on seismic faults in the crust or plates and lead to trigger other earthquakes (Sibson et al., 1975; Sibson, 1981; Hickman et al., 1995). Among them, we examine the Coulomb stress changes caused by large earthquakes as a triggering mechanism of nearby large earthquakes, because many various case studies support the static stress change as one of the most probable earthquake triggering mechanism (Hardebeck et al. 1998; Toda et al. 2008, 2011; Ishibe et al. 2017).

The change of Coulomb failure function (ΔCFF) is defined as $\Delta CFF = \Delta\tau + \mu'\Delta\sigma$, where $\Delta\tau$ is the shear stress change, $\Delta\sigma$ is the normal stress change and μ' is the apparent coefficient of friction [e.g., Reasenberg and Simpson, 1992]. We calculate ΔCFF for two nodal planes of a slave event by using a moment tensor solution of its master event. We calculate ΔCFF using Coulomb3.3 program provided by USGS (https://www.usgs.gov/software/coulomb-3). Since Global CMT catalog only provides a moment tensor solution assuming a point source, we assume an appropriate fault length, L, and width, W, of a master event by using an empirical relation on the magnitude and fault size presented in Wells and Coppersmith (1994): $L = 10^{-3.22+0.69*M_w}$ and $W = 10^{-1.01+0.32*M_w}$. We make all calculations in an elastic half-space with a shear modulus $3.2\text{x}10^4$ MPa, a Poisson's ratio of 0.25 and

μ' = 0.4. The source is assumed to be the master event of each cluster and the receivers are all slave events belonging to that cluster. We only analyze the earthquakes with magnitude of larger than 6.

Figure 7 shows the frequency distributions of ΔCFF for the three magnitude ranges calculated on the two candidate fault planes. Most of the ΔCFF are distributed around 0 Pa, but positive ΔCFF tends to be distributed in a wider range than negative ones. The percentages of positive ΔCFF for the first fault plane are 80% for $6.0 \leq M_w < 6.5$, 69% for $6.5 \leq M_w < 7.0$ and 60% for $M_w \geq 7.0$, respectively, and those for the second fault plane 77%, 72%, and 62%, respectively. This result suggest that Coulomb stress change may play a role on the generation of triggered earthquakes. However, when 10^3Pa is used as a threshold stress for triggering successive earthquakes, which is the same order of the stress perturbation generated from the solid earth tide that may trigger earthquakes (e.g., Tanaka et al., 2002a and 2002b), the percentage of the slave events that satisfy the triggering condition decrease down to about 40 to 45 % for the magnitude ranges of larger than 6.

About 27 % of slave events occurred in the region with negative ΔCFF. Also, the triggering distances decreases with lapse time. These may not be explained by the triggering mechanism of static stress changes caused by master events. Triggering mechanism of, for example, dynamic stress (strong motion) by main shock, slower deformation processes due to visco-elastic behavior in crust and mantle, and the ambient stress field due to plate tectonic motion, or unknown process may explain such triggering.

5. Conclusion

We have systematically examined the spatio-temporal clustering of earthquakes after the occurrence of a moderate or large earthquake by analyzing one of the most reliable modern seismic data catalog of centroid moment tensor solutions. We examined the number of earthquakes that closely occurred in a space and time from master earthquakes and compare the results with those obtained from the simulated data in which the earthquakes randomly occur in time. The results show that the large earthquakes trigger nearby large earthquakes beyond so called aftershock areas. The triggered earthquakes are about 5 to 40 % of all the earthquakes for the magnitude ranges of $5 \leq M_w < 9.5$, which are distributed not only along subduction zones but also along rift zones. Triggering distances, which defines the distance from the master earthquake to triggered earthquakes, increase with increasing the magnitude of master earthquake, and decrease with increasing the lapse time. The triggering distance increases with being proportional to the 1/3 of the seismic moment of master earthquakes. More than 60% of the triggered earthquakes occur in the region with positive ΔCFF caused by master event. These results suggest that static stress changes may generate successive large earthquakes. The estimated percentages of the successive earthquakes for magnitude range and

horizontal distance from the master large earthquake can be used for evaluating an occurrence possibility of next large earthquakes.

Abbreviations

CMT: Centroid moment tensor; ETAS: Epidemic type aftershock sequence; CFF: Coulomb failure function.

Acknowledgement

We thank Professor Shinji Toda (Tohoku University) for his suggestive comments that improve the manuscript. We use CMT solutions provided by Colombia university.

Authors' contributions

TMB performed data analyses with TN. Both authors discussed the results and contributed to the paper writing. Both authors read and approved the final manuscript.

Funding

This study was supported by the Graduate School of Science, Tohoku University.

Availability of data and materials

The data catalog of centroid moment tensor (CMT) solutions analyzed in the current study are available via (www.globalcmt.org). We use Coulomb3.3 program to calculate the change in Coulomb failure function (ΔCFF) that is available via (https://www.usgs.gov/software/coulomb-3).

Competing interests

The authors declare that they have no competing interests.

References

Bak P K (2002) Unified scaling law for earthquakes. Phys Rev Lett 88 (17):178501. doi: 10.1103/PhysRevLett.88.178501.

Bath M (1965) Lateral inhomogeneities in the upper mantle. Tectonophysics 2:483 – 514.

Bormann P, Giacomo D (2010) The moment magnitude and the energy magnitude: common roots and differences. J Seismology 15:411-427. doi:10.1007/s10950-010-9219-2.

Console R, Murru M (2001) A simple and testable model for earthquake clustering. J Geophys Res 166: 8699- 8711.

361 Corral Á (2004a) Long-term clustering, scaling, and universality in the temporal occurrence of
362 earthquakes. Phys Rev Lett 92 (10):108501. doi: 10.1103/ PhysRevLett.92.108501.

363 Corral Á (2004b) Universal local versus unified global scaling laws in the statistics of seismicity.
364 Physica A 340 (4):590-597. doi: 10.1016/j.physa.2004.05.010.

365 Corral Á (2008) Scaling and universality in the dynamics of seismic occurrence and beyond. In:
366 Carpinteri A, Lacidogna G (eds.) Acoustic Emission and Critical Phenomena, Taylor & Francis
367 Group, London, pp 225-244. doi: 10.1201/9780203892220.ch2.2.

368 Davidsen J, Paczuski M (2005) Analysis of the spatial distribution between successive earthquakes,
369 Phys Rev Lett 94 (4):048501. doi: 10.1103/PhysRevLett.94.048501.

370 Dziewonski AM, Chou TA, Woodhouse JH (1981) Determination of earthquake source parameters
371 from waveform data for studies of global and regional seismicity. J Geophys Res 86:2825-2852.
372 doi:10.1029/JB086iB04p02825.

373 Ekström G, Nettles M, Dziewonski AM (2012) The global CMT project 2004-2010: Centroid-moment
374 tensors for 13,017 earthquakes. Phys Earth Planet Inter 200:1-9. doi:
375 10.1016/j.pepi.2012.04.002.

376 Felzer KR, Brodsky EE (2006) Decay of aftershock density with distance indicates triggering by
377 dynamic stress. Nature 441: 735–738. doi:10.1038/nature04799.

378 Freed AM, Lin J (2001) Delayed triggering of the 1999 Hector Mine earthquake by viscoelastic stress
379 transfer. Nature 411:180–183.

380 Freed MA (2005) Earthquake triggering by static, dynamic, and postseismic stress transfer. Annu Rev
381 Earth Planet Sci 33:335–67. doi: 10.1146/annurev.earth.33.092203.122505.

382 Goda K, Campbell G, Hulme L, Ismael B, Ke L, Marsh R, Sammonds P, So E, Okumura Y, Kishi N,
383 Yotsui S, Kiyono J, Wu S, Wilkinson S (2016) The 2016 Kumamoto earthquakes: Cascading
384 Geological Hazards and Compounding Risks. Front Built Environ 2:19. doi:
385 10.3389/fbuil.2016.00019.

386 Gomberg J, Beeler NM, Blanpied ML, Bodin P (1998) Earthquake triggering by transient and static
387 deformations. J Geophys Res 103(B10):24,411–24,426. doi:10.1029/98JB01125.

388 Gomberg J, Johnson P (2005) Dynamic triggering of earthquakes. Nature 437(7060):830. doi:
389 10.1038/437830a.

390 Gutenberg B, Richter C (1944) Frequency of earthquakes in California. Bull Seismol Soc Am 34:185
391 – 188.

392 Hanks C, Kanamori H (1979) A moment magnitude scale. J Geophys Res 84:2348- 2350.

393 Hardebeck J L, Nazareth JJ, Hauksson E (1998) The static stress change triggering model: Constraints
394 from two southern California aftershock sequences. J Geophys Res 103(B10):24,427–24,437.
395 doi:10.1029/98JB00573.

396 Helmstetter A, Sornette D (2002) Subcritical and supercritical regimes in epidemic models of
397 earthquake aftershocks. J Geophys Res 107:2237. doi 10.1029/2001JB001580.

398 Helmstetter A, Sornette D (2004) Comment on "Power-law time distribution of large earthquakes".
399 Phys Rev Lett. doi: 10.1103/ PhysRevLett.92.129801.

400 Hickman S, Sibson R, Bruhn R (1995) Introduction to special section: Mechanical involvement of fluids
401 in faulting. J Geophys Res, 100:12,831–12,840. doi:10.1029/95JB01121.

402 Hill DP, Reasenberg PA, Michael A, Arabaz WJ, Beroza G, Brumbaugh D, Brune JN, Castro R, Davis
403 S, dePolo D, Ellsworth WL, Gomberg J, Harmsen S, House L, Jackson SM, Johnston MJS,
404 Jones L, Keller R, Malone S, Munguia L, Nava S, Pechmann JC, Sanford A, Simpson RW,
405 Smith RB, Stark M, Stickney M, Vidal A, Walter S, Wong V, Zollweg J (1993) Seismicity
406 remotely triggered by the magnitude 7.3 Landers, California, earthquake. Science 260:1617–
407 1623. doi:10.1126/science.260.5114.1617.

408 Ishibe T, Ogata Y, Tsuruoka H, Satake K (2017) Testing the Coulomb stress triggering hypothesis for
409 three recent megathrust earthquakes. Geosci Lett 4:5. doi 10.1186/s40562-017-0070-y.

410 Kagan YY, Knopoff L (1980) Spatial distribution of earthquakes: the two-point correlation function.
411 Geophys J Int 62:303-320. doi.org/10.1111/j.1365-246X.1980.tb04857.x.

412 Kanamori H, Anderson DL (1975) Theoretical basis of some empirical relationships in seismology.
413 Bull Seismol Soc Am 65:1073-1095.

414 Kilb D, Gomberg J, Bodin P (2000) Triggering of earthquake aftershocks by dynamic stresses. Nature
415 408(6812):570-4. doi:10.1038/35046046.

416 King GCP, Stein RS, Lin J (1994) Static stress changes and triggering of earthquakes. Bull Seismol Soc
417 Am 84 (3):935 – 953.

418 Kumazawa T, Ogata Y (2014) Nonstationary ETAS models for nonstandard earthquakes. Ann Appl
419 Stat 8(3):1825–1852. doi:10.1214/14-AOAS759.

420 Marekova E (2014) Analysis of the spatial distribution between successive earthquakes occurred in
421 various regions in the world. Acta Geophysica. doi: 10.2478/s11600-014-0234-5.

422 Marson D, Lengline O (2010) A new estimation of the decay of aftershock density with distance to
423 mainshock. J Geophys Res. doi:10.1029/2009JB007119.

424 Marson D, Enescu B (2012) Modeling the foreshock sequence prior to the 2011, MW9.0 Tohoku, Japan,
425 earthquake. J Geophys Res 117:B06316. doi:10.1029/2011JB009039.

426 Michael AJ (2011) Random variability explains apparent global clustering of large earthquakes.
427 Geophys Res Letters. doi: 10.1029/2011GL049443.

428 Neves M. Custódio S, Peng Z, Ayorinde A (2018) Earthquake triggering in southeast Africa following
429 the 2012 Indian Ocean earthquake. Geophys J Int 212:1331–1343. doi: 10.1093/gji/ggx462.

430 Nicole D. et al., (2018) Spatiotemporal Analysis of the Foreshock– Mainshock–Aftershock Sequence
431 of the 6 July 2017 Mw 5.8 Lincoln, Montana, Earthquake. Seismol Res Lett 90 (1): 131-139.
432 doi.org/10.1785/0220180180**.**

433 Nishimura T (2017) Triggering of volcanic eruptions by large earthquakes. Geophys Res Lett 44:7750–
434 7756. https://doi.org/10.1002/ 2017GL074579.

435 Ogata Y (1998) Space–time point-process models for earthquake occurrences. Ann Inst Stat Math 50:
436 379 – 402.

437 Ogata Y, Zhuang (2006) Space–time ETAS models and an improved extension. Tectonophysics
438 413:13–23.

439 Pollitz FF, Stein RS, Sevilgen V, Bûrgmann R (2012) The 11 April 2012 east Indian Ocean earthquake
440 triggered large aftershocks worldwide. Nature 490:250–253. doi:10.1038/nature11504.

441 Reasenberg PA, Simpson RW (1992) Response of regional seismicity to the static stress change
442 produced by the Loma Prieta earthquake. Science 255:1687–1690.

443 Reasenberg PA (1999) Foreshock occurrence before large earthquakes. J Geophys Res 104 (B3):4755-
444 4768.

445 Richards-Dinger K, Stein RS, Toda S (2010) Decay of aftershock density with distance does not indicate
446 triggering by dynamic stress. Nature 467:583–586. https://doi.org/10.1038/nature09402.

447 Shearer PM, Stark PB (2012) Global risk of big earthquakes has not recently increased. Proc Nat Acad
448 Sci USA 109 (3):717-721. doi: 10.1073/pnas.1118525109.

449 Sibson RH, Moore JMcM, Rankin AH (1975) Seismic pumping: A hydrothermal fluid transport
450 mechanism. J Geol Soc London 131:652–659.

Sibson RH (1981) Fluid flow accompanying faulting: Field evidence and models, Earthquake Prediction. In: International Review (ed Simpson DW, Richards PG). Am Geophys Union, Maurice Ewing Series 4, pp 593-603.

Stein RS (1999) The role of stress transfer in earthquake occurrence. Nature 402(6762):605–609.

Tamaribuchi K, Yagi Y, Enescu B, Hirano S (2018) Characteristics of foreshock activity inferred from the JMA earthquake catalog. Earth Planets Space 70:90. doi.org/10.1186/s40623-018-0866-9.

Tanaka S, Ohtake M, Sato H (2002a) Spatio-temporal variation of the tidal triggering effect on earthquake occurrence associated with the 1982 South Tonga earthquake of Mw 7.5. Geophys Res Lett 29 (16):1756. doi:10.1029/2002GL015386.

Tanaka S, Ohtake M, Sato H (2002b) Evidence for tidal triggering of earthquakes as revealed from statistical analysis of global data. J Geophys Res 107 (B10): 2211. doi:10.1029/2001JB001577.

Toda S, Lin J, Meghraoui M, Stein RS (2008) 12 May 2008 M=7.9 Wenchuan, China, earthquake calculated to increase failure stress and seismicity rate on three major fault systems. Geophys Res Lett 35:L17305. doi:10.1029/2008GL034903.

Toda S, Stein RS, Lin J (2011) Widespread seismicity excitation throughout central Japan following the 2011 M=9.0 Tohoku earthquake and its interpretation by Coulomb stress transfer. Geophys Res Lett 38:L00G03. doi:10.1029/2011GL047834, 201.

Toda S, Stein RS, Sevilgen V, Lin J (2011a) Coulomb 3.3 Graphic-rich deformation and stress-change software for earthquake, tectonic, and volcano research and teaching-user guide. U.S. Geological Survey. Open-File Report 2011–1060. https://pubs.usgs.gov/of/2011/1060/of2011-1060.pdf. Accessed 21 Feb 2017.

Toda S, Lin J, Stein RS (2011) Using the 2011 Mw 9.0 off the Pacific coast of Tohoku earthquake to test the Coulomb stress triggering hypothesis and to calculate faults brought closer to failure. Earth Planets Space 63:725–730. doi:10.5047/eps.2011.05.010.

Utsu T, Seki A (1954) A relation between the area of after-shock region and the energy of main-shock. J Seismol Soc Jpn 7:233-240 (in Japanese with English abstract).

Utsu T (1957) Magnitude of earthquakes and occurrence of their aftershocks. J Seismol Soc Jpn 10:35 - 45 (in Japanese with English abstract).

Utsu T, Ogata Y, Matsu'ura R (1995) The centenary of the Omori formula for a decay law of aftershocks activity. J Phys Earth 43 (1):1–33. doi: 10.4294/jpe1952.43.1.

Utsu T (2002) Statistical features of seismicity. In Lee WHK (ed) International Handbook of Earthquake & Engineering Seismology Part A. Academic, San Diego, pp 719–73.

Wells DL, Coppersmith KJ (1994) New Empirical Relationships among Magnitude, Rupture Length, Rupture Width, Rupture Area, and Surface Displacement. Bull Seismol Soc Am 84 (4):974-1002.

Yukutake Y, Lio Y (2017) Why do aftershocks occur? Relationship between mainshock rupture and aftershock sequence based on highly resolved hypocenter and focal mechanism distributions. Earth Planets Space 69:68. doi: 10.1186/s40623-017-0650-2.

Figure Legends

Figure 1. Schematic illustration of the selection method of master event and the removal of the aftershocks. We sort the earthquake catalog in time, and we select the first earthquake as a master event in a given magnitude range. We then find slave events and select a next master event from the catalog and repeat these process. q_1 is the first master event (E_0^1), and q_2 is its slave event. q_3 is out of the magnitude range so that this is not selected as a master event. q_4 is not selected as a mater event, because it occurs within 2000 km distance and $t_b \leq 14$ days from a larger earthquake, q_3. q_5 is selected as master event (E_0^2) because it occurs at distance larger than 2000 km from a larger earthquake q_3 even though within $t_b \leq 14$ days (but withtout no slave event). q_6 is an earthquake out of target magnitude. q_7 is not selected as a master event because it is close to q_6. q_8 is selected as master event (E_0^3) because it is larger than q_7 even though occurs within 2000 km distance and $t_b \leq 14$ days from q_7. q_9 is also selected as master event (E_0^4) because it occurs at a distance larger than 2000km and $t_b > 14$ days from a larger earthquake, q_6, and q_{10} is its slave event.

Figure 2. Schematic illustrations to show how different clusters of successive earthquakes are defined for different choices of D and T_a. Blue circles represent master events, gray circles slave events and each gray ellipse indicates a group of successive earthquakes (clusters). (a) A group of clusters obtained for initial D and T_a. To remove aftershock activity, we do not use the earthquakes (S_i) occurring within a distance of D_{min} that is determined from the magnitude of master event. (b) Green circle and green ellipse represent new slave events and a new cluster, respectively, obtained by increasing D. (c) Orange circle and orange ellipse represent a new slave event and a new cluster, respectively, obtained by increasing T_a. (d) New slave events and new clusters obtained by increasing both D and T_a.

Figure 3. Cumulative numbers of the observed (solid lines) and simulated (dotted lines) clusters versus horizontal distance for three lapse times (c=3 and $t_b = 14$ day. Note that the ranges of vertical axis are different for (a) – (e). Arrows indicate the triggering distances where the cumulative numbers of the observed and simulated clusters merge (see text).

Figure 4. Relationships between the triggering distances and seismic moment. Triggering distances are measured for different parameters t_b (a) and c (b).

Figure 5. Spatial distributions of the successive earthquakes determined for (a) $Mw \geq 7.0$ (b) $6.5 \leq Mw < 7.0$, and (c) $6.0 \leq Mw < 6.5$. Blue, orange, maroon colors represent the successive earthquakes occurring within distances of 100, 500 and 1000 km, respectively, within a lapse time of 180 days.

Figure 6. Frequency distributions of the triggering distances calculated for 100 simulated data. The observed triggering distances measured from the average of the simulation are indicated by red dotted lines. Two lapse times (T_a) are examined: (a,b,c) for 365 days and (d,e,f) for 180 days.

Figure 7. Frequency distribution of Coulomb stress change calculated for the first fault plane (a,b,c) and the second one (d,e,f). Solid and dotted red lines indicate $\Delta\mathrm{CFF}$ of 0 Pa and 10^3 Pa, respectively.

Table Legends

Table 1. Successive earthquakes within triggering distance.

Figures

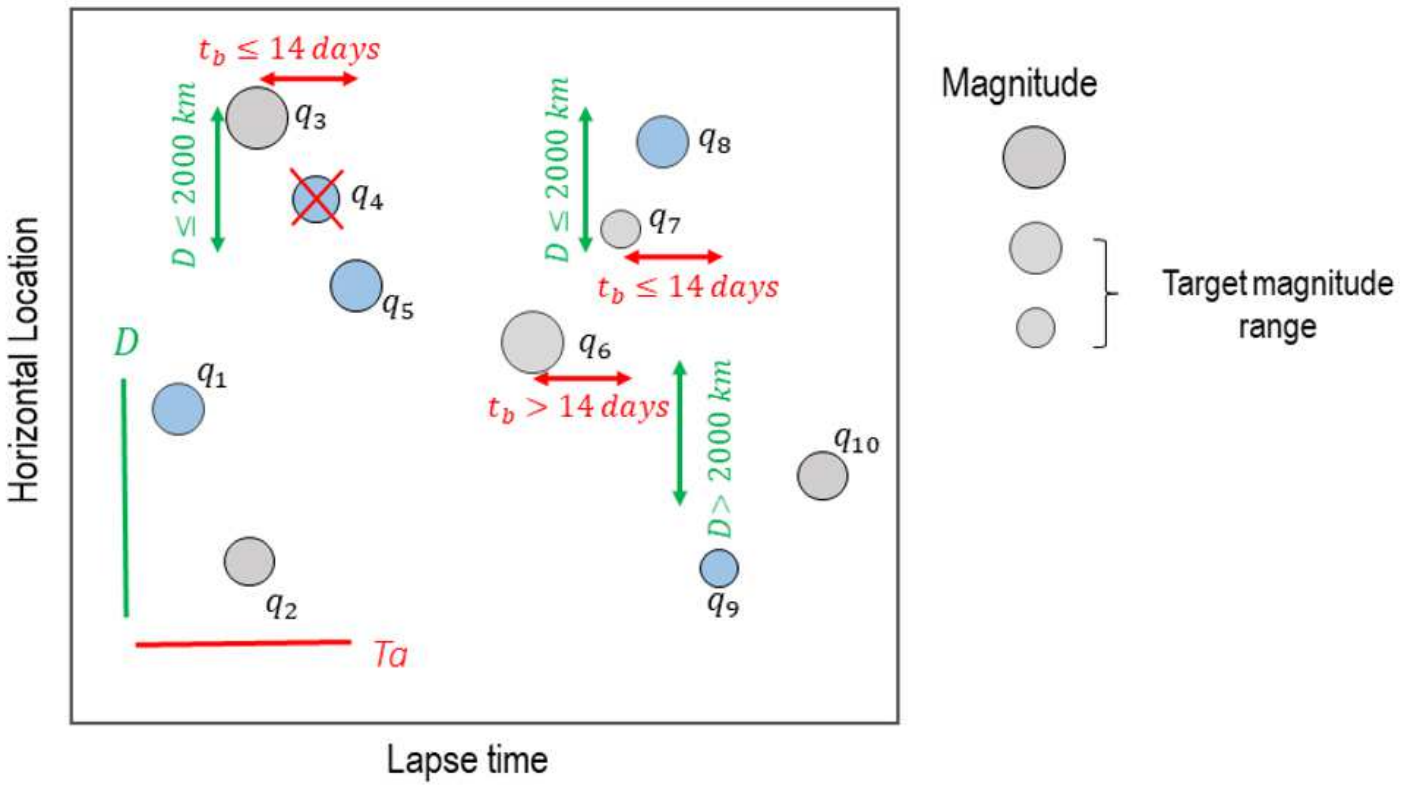

Figure 1

Schematic illustration of the selection method of master event and the removal of the aftershocks. We sort the earthquake catalog in time, and we select the first earthquake as a master event in a given magnitude range. We then find slave events and select a next master event from the catalog and repeat these process. q_1 is the first master event (E_0^1), and q_2 is its slave event. q_3 is out of the magnitude range so that this is not selected as a master event. q_4 is not selected as a mater event, because it occurs within 2000 km distance and t_b≤14 days from a larger earthquake, q_3. q_5 is selected as master event (E_0^2) because it occurs at distance larger than 2000 km from a larger earthquake q_3 even though within t_b≤14 days (but withtout no slave event). q_6 is an earthquake out of target magnitude. q_7 is not selected as a master event because it is close to q_6. q_8 is selected as master event (E_0^3) because it is larger than q_7 even though occurs within 2000 km distance and t_b≤14 days from q_7. q_9 is also selected as master event (E_0^4) because it occurs at a distance larger than 2000km and t_b>14 days from a larger earthquake, q_6, and q_10 is its slave event.

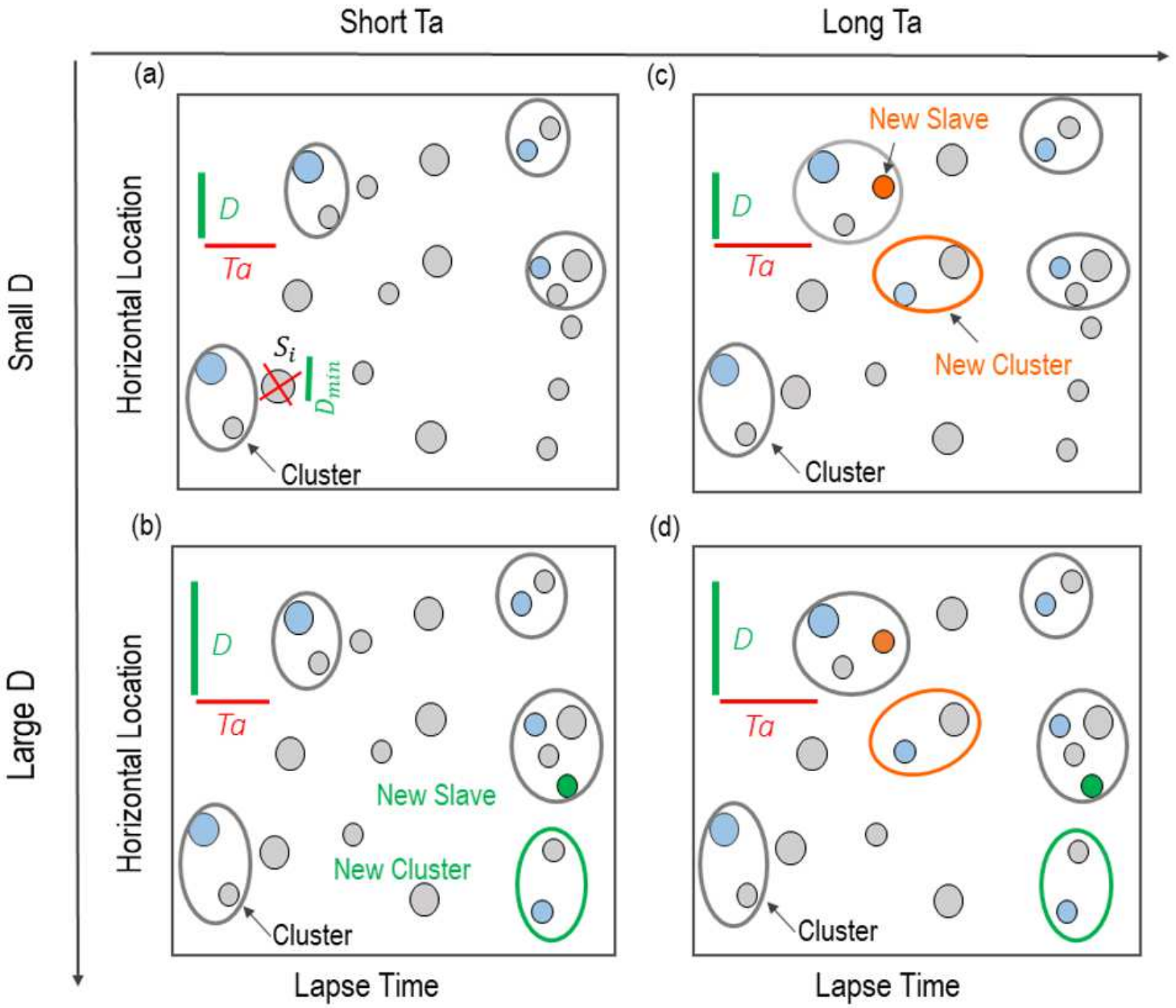

Figure 2

Schematic illustrations to show how different clusters of successive earthquakes are defined for different choices of D and T_a. Blue circles represent master events, gray circles slave events and each gray ellipse indicates a group of successive earthquakes (clusters). (a) A group of clusters obtained for initial D and T_a. To remove aftershock activity, we do not use the earthquakes (S_i) occurring within a distance of D_min that is determined from the magnitude of master event. (b) Green circle and green ellipse represent new slave events and a new cluster, respectively, obtained by increasing D. (c) Orange circle and orange ellipse represent a new slave event and a new cluster, respectively, obtained by increasing T_a. (d) New slave events and new clusters obtained by increasing both D and T_a.

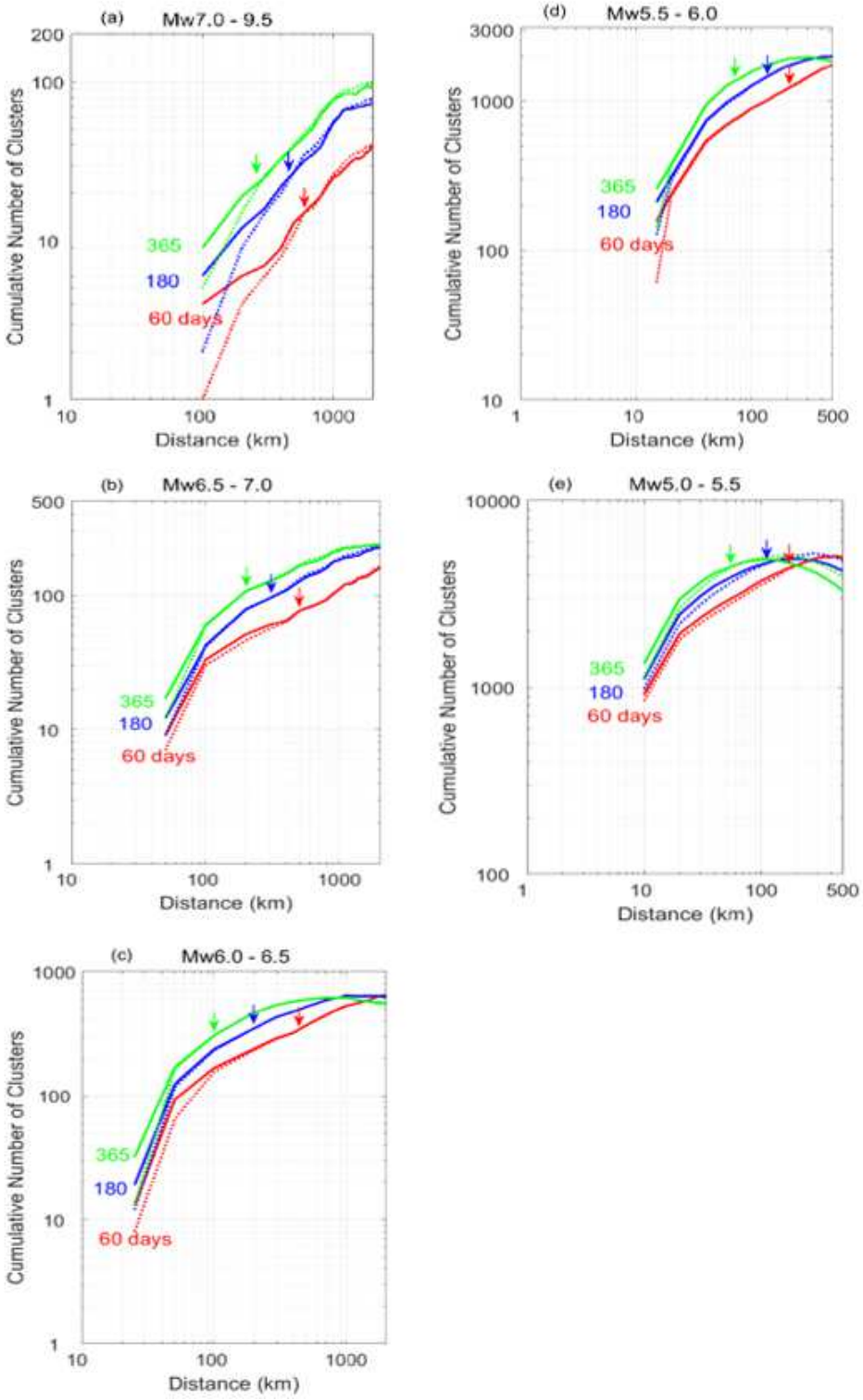

Figure 3

Cumulative numbers of the observed (solid lines) and simulated (dotted lines) clusters versus horizontal distance for three lapse times (c=3 and t_b=14 day. Note that the ranges of vertical axis are different for (a) – (e). Arrows indicate the triggering distances where the cumulative numbers of the observed and simulated clusters merge (see text).

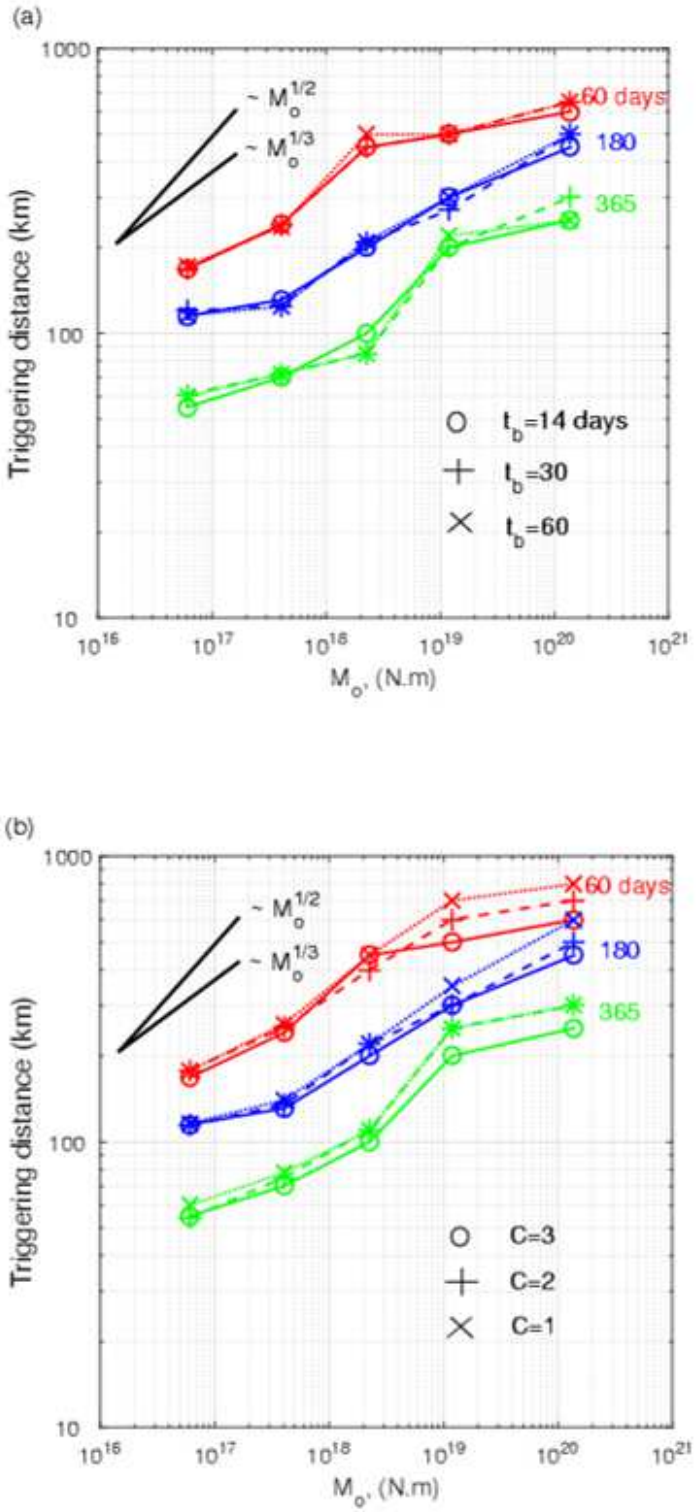

Figure 4

Relation between triggering distances and seismic moment. Triggering distances are measured for different parameters t_b (a) and c (b).

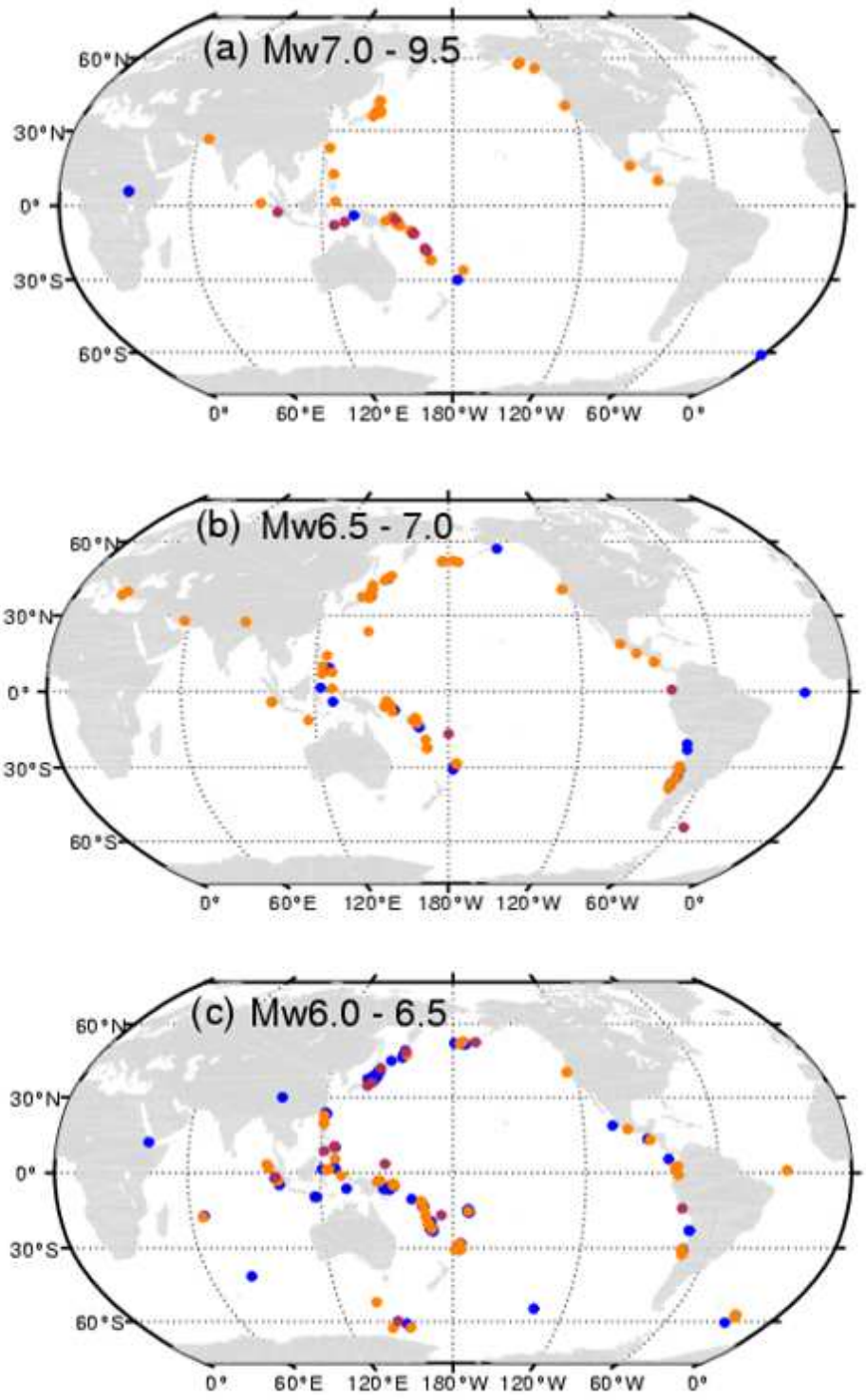

Figure 5

Spatial distributions of the successive earthquakes determined for (a) Mw≥7.0 (b) 6.5≤Mw<7.0, and (c) 6.0≤Mw<6.5. Blue, orange, maroon colors represent the successive earthquakes occurring within distances of 100, 500 and 1000 km, respectively, within a lapse time of 180 days.

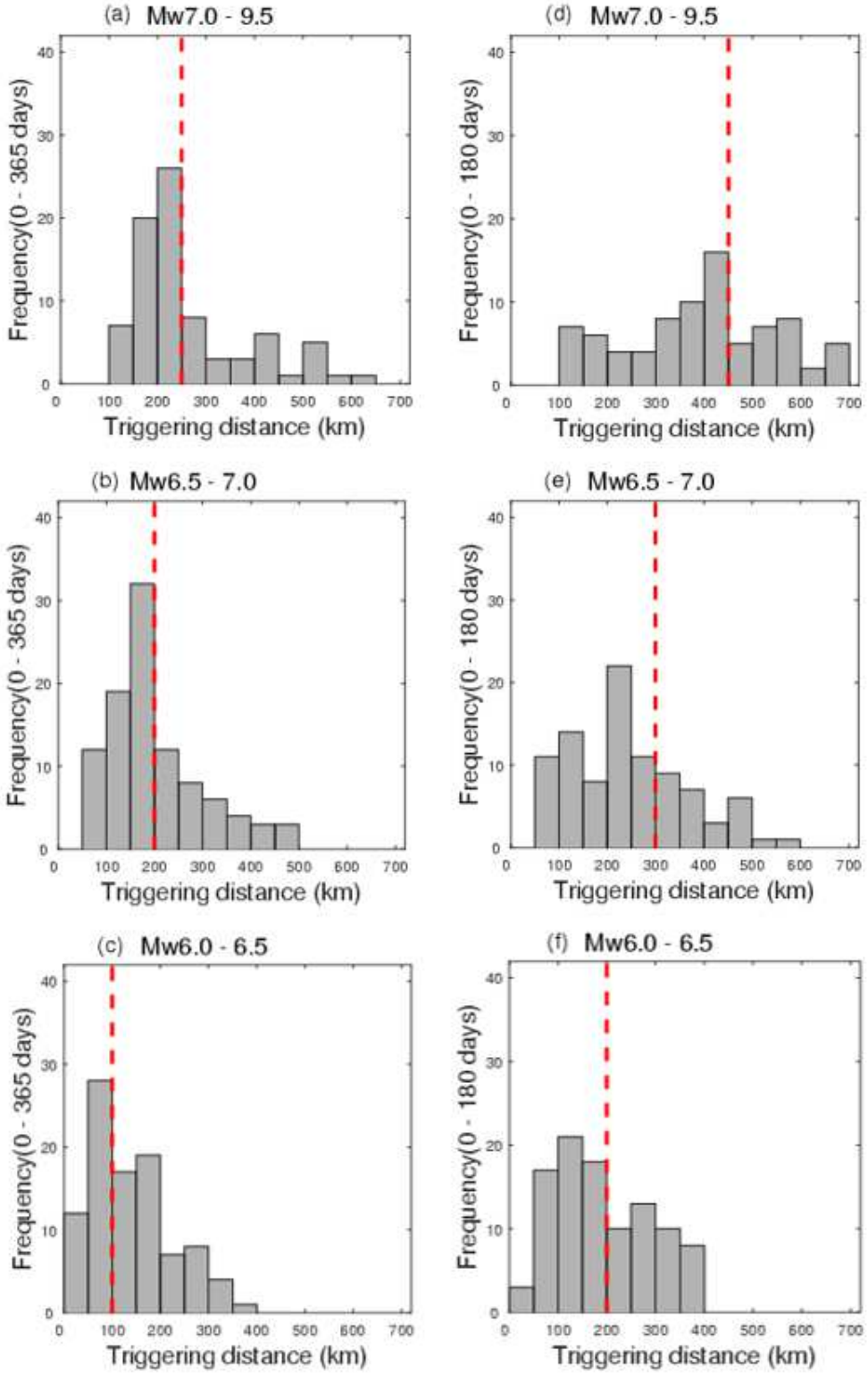

Figure 6

Frequency distributions of the triggering distances calculated for 100 simulated data. The observed triggering distances measured from the average of the simulation are indicated by red dotted lines. Two lapse times (T_a) are examined: (a,b,c) for 365 days and (d,e,f) for 180 days.

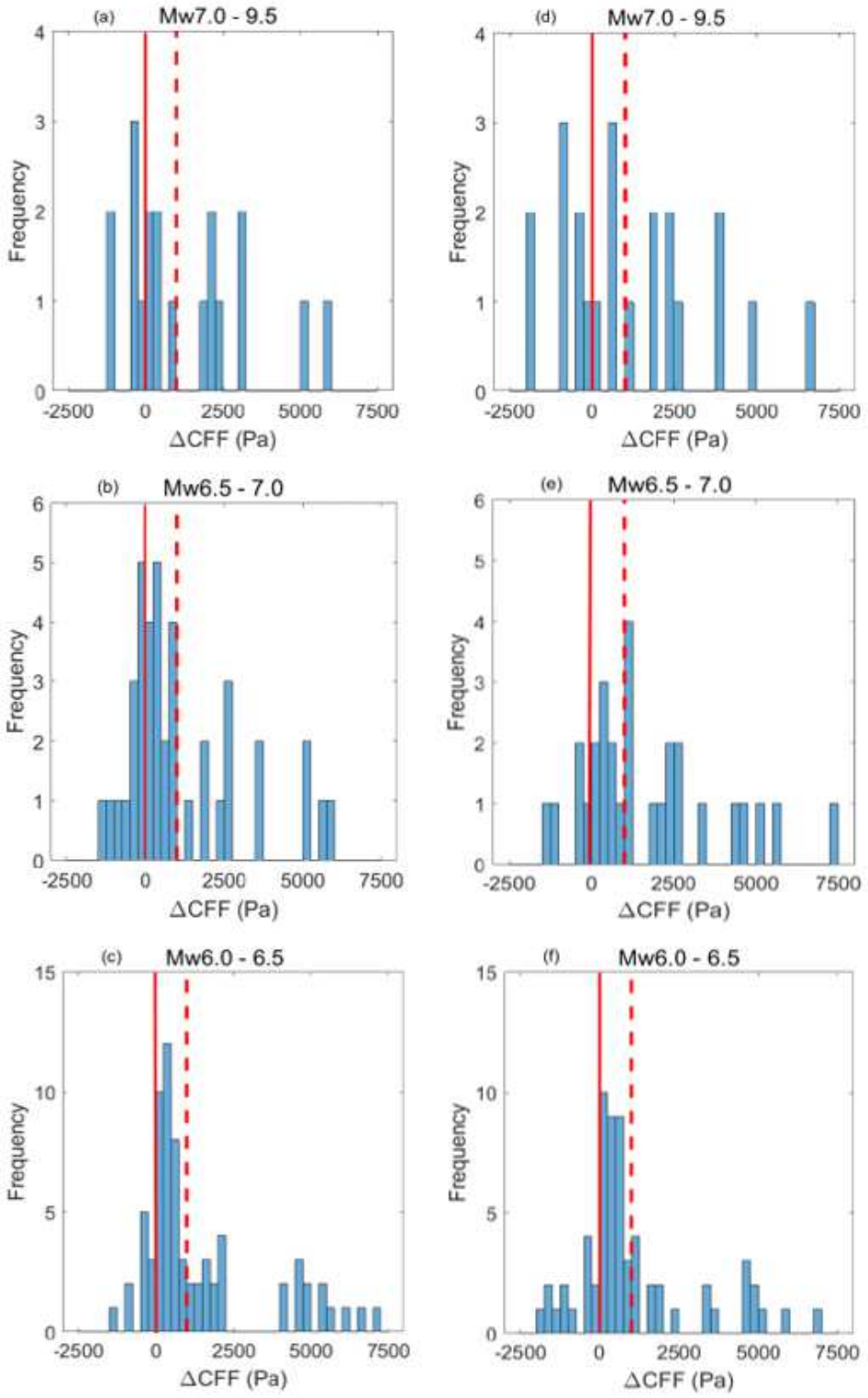

Figure 7

Frequency distribution of Coulomb stress change calculated for the first fault plane (a,b,c) and the second one (d,e,f). Solid and dotted red lines indicate ΔCFF of 0 Pa and 10^3 Pa, respectively.

Supplementary Files

This is a list of supplementary files associated with this preprint. Click to download.

- Graphicalabstract.png